Hindawi
Laser and Particle Beams
Volume 2022, Article ID 4546178, 10 pages
https://doi.org/10.1155/2022/4546178

Research Article

Fabrication and Optimization Design of Multilayer Flyer Plates for Laser-Driven Loading

Wei Guo ,[1] Wei Cao ,[1] Xiang Wang,[1] Qiqi Peng,[2] and Lizhi Wu[3]

[1]*Institute of Chemical Materials, China Academy of Engineering Physics, Mianyang 621999, China*
[2]*Shaanxi Applied Physics-Chemistry Research Institute, Xi'an 710061, China*
[3]*Department of Chemical Engineering, Nanjing University of Science and Technology, Nanjing 210094, China*

Correspondence should be addressed to Wei Guo; guoweizmf@njust.edu.cn

Received 19 September 2021; Revised 6 December 2021; Accepted 18 December 2021; Published 3 March 2022

Academic Editor: Daniele Margarone

The laser-driven flyer plate is an important loading technology in high energy physics, shock wave physics, and explosive initiation application. How to generate a high-velocity and intact flyer plate by using the laser is a matter of concern for laser driving. In this study, the multilayer flyer plates (MFPs) of $Al/Al_2O_3/Al$ and $TiO_2/Al/Al_2O_3/Al$ with adjustable performance were designed and fabricated by magnetron sputtering and analyzed by scanning electron microscopy (SEM), laser reflectance spectrometer, and differential thermal analysis (DTA). The effects of the structure and material on the output performance of MFPs were analyzed by photon Doppler velocimetry (PDV) and ultrahigh-speed video. The morphology results showed that the structure of MFPs had uniform and clear boundaries between side-by-side layers. The MFP velocity was controlled in the range of 4.0–6.0 km/s by adjusting the film thickness, structure, and thermite material with 43.1 J/cm^2 laser ablation. Among them, the energetic flyers with the thermite ablation layer had the highest final velocity of 5.38 km/s due to the prestored energy of TiO_2/Al. By appropriately increasing the thickness of Al_2O_3 from 0.4 μm to 0.8 μm, the complete flight of the flyer plate to 3.72 mm can be realized. In addition, TiO_2/Al thermite film had characteristics of reaction heat release and lower laser reflectivity (72.13%) than the Al layer (80.55%), which explained the velocity enhancement effect of energetic flyer plates. This work provides facile strategy to enhance the output performance of MFPs, which may facilitate the practical applications of laser driving technology.

1. Introduction

Laser-driven flyer plate is an important dynamic high-pressure loading method, the main principle of which is the utilization of a high-power pulse laser to ablate film to form plasma. High-temperature and high-pressure plasma expands to drive the remaining film to fly at high speed, thereby achieving output work through the high-speed flyer plate hitting the target. Laser-driven flyer plate was originally proposed by Krehl from Sandia National Laboratories in the United States [1]. It is an effective technology to obtain the flyer plate with high speed and high impact pressure and has the characteristics of low cost and simple installation [2–6]. In the 1980s, Paisley realized the impact initiation of fine-grained HNS by using the laser-driven flyer plate for the first time and started the impact initiation of insensitive explosives by using the laser as energy [7]. In order to realize the miniaturization and engineering application of the laser-driven flyer plate impact initiation, many researchers have carried out a wealth of research from the aspects of optical fiber transmission of pulsed laser energy, preparation of high-efficiency flyer plates, and refinement of detonating agents [8–15]. Bowden et al. developed a laser-driven flyer initiation system under the condition of closed optical path by using the optical fiber transmission laser [16]. Chen et al. used magnetron sputtering to prepare multilayer flyer plates (MFPs) with the Al_2O_3 insulation layer, which effectively reduced the initiation threshold of HNS-IV by the laser-driven flyer plate [17, 18]. Wu et al. used the thermite film as the ablative layer structure of the MFPs and increased the flyer velocity by about 10% [19, 20]. Among them, improving the output performances of the plasma-driven flyer plate formed by the laser-ablated film has always been a research hotspot, and higher laser-driven flyer velocity and more complete flyer morphology are the goals pursued by researchers.

Previously, the energetic flyer plates were prepared with different thermite-ablative layers [21, 22], and the flyer plates with excellent performance were obtained, but the effects of thicknesses and structures on the performance of flyer plates were explored less, especially compared with the non-energetic flyer plate. This study focused on changing the thicknesses of layers (ablative layer/insulation layer/flyer layer), compared with previous studies that only changed the material but fixed the thickness of each layer. Therefore, by adjusting the thicknesses of the ablation and insulation layer from 0.4 μm to 0.8 μm and the thickness of the flyer layer from 2.6 μm to 3.2 μm, three MFPs of $Al/Al_2O_3/Al$ (I), $Al/Al_2O_3/Al$ (II), and $TiO_2/Al/Al_2O_3/Al$ (III) were prepared. The velocity and morphology of the flyer plates were characterized by the photonic Doppler velocimetry (PDV) system and ultrahigh-speed video. The characteristics of flyers with different film structures and thicknesses were evaluated by observing and analyzing the fragmentation and decomposition (through the increase process of the flyer velocity and the change process of the flyer morphology) under the action of plasma erosion, which has not been paid much attention in previous studies on laser-driven flyers. In addition, thermal analysis and reflectance analysis showed the energy enhancement effect of energetic films by using the laser. By adjusting the thickness of each layer of the flyer film, the influence of the film layer on the performance of the flyer was obtained, which provided a design scheme for the laser flyer plate. The acceleration process and mechanism of MFPs with different structures driven by using the laser were analyzed in depth, so as to provide support for the design and application of MFPs with high output performance.

2. Experimental Section

2.1. Laminate Preparation. The nonenergetic $Al/Al_2O_3/Al$ (ablative layer/insulation layer/flyer layer) and energetic $TiO_2/Al/Al_2O_3/Al$ (ablative layer/ablative layer/insulation layer/flyer layer) laminates were deposited on a K9 substrate ($\Phi 5\,mm \times 2\,mm$) by magnetron sputtering. The impurities such as oil and dust on the K9 glass surface were cleaned with alcohol, acetone, and deionized water, respectively. Then, the cleaned K9 glass was placed in the vacuum chamber of the coating machine, and the MFPs with different film thicknesses were accurately prepared by the radiofrequency (RF) magnetron sputtering technique. The Al target disk ($\Phi 50\,mm \times 4\,mm$, purity >99.999%), TiO_2 target disk ($\Phi 50\,mm \times 4\,mm$, purity >99.99%), and Al_2O_3 target disk ($\Phi 50\,mm \times 4\,mm$, purity >99.99%) were purchased from Zhongnuo Xincai Technology Corporation and used for depositing Al, TiO_2, and Al_2O_3 films. The power delivered to the discharge was 229 W (TiO_2 target), 234 W (Al_2O_3 target), and 204 W (Al target), respectively. The pressure in the vacuum chamber was pumped away below 3×10^{-3} Pa before deposition. Then, ultrahigh-purity argon (99.999%) was passed into the chamber as the working gas with a flux of 30 sccm to keep the working pressure at 0.4 Pa. The multilayer films were deposited alternately on K9 glass by rotating the substrate tray. The morphologies of the $Al/Al_2O_3/Al$ and $TiO_2/Al/Al_2O_3/Al$ laminates were analyzed using scanning electron microscopy (SEM). Laser reflectivity and heat release were characterized by using the laser reflectance spectrometer and differential thermal analysis (DTA and TA Instruments SDT600), respectively.

2.2. Drive Test of MFPs. A pulsed laser (6.5 ns, 1064 nm) system (it mainly consisted of a laser system, two retroreflectors, and a lens with a focal length of 20 cm) was performed to test the drive characteristics of MFPs, which is illustrated in Figure 1. The flight velocity curves and flight process photos were characterized by the PDV system and an ultrahigh-speed camera (Specialized Imaging, SIMD16), respectively. Solid pulsed Q-switched Nd : YAG (1064 nm, 6.5 ns) output a Gaussian laser pulse through a convex lens in an atmosphere environment. In the experiment, a Gaussian short-pulse laser was produced, and a convex lens focused the beam, and then, the surface of the MFPs was irradiated. At the same time, the velocity signal was recorded by the PDV system, and the drive process of the MFP was recorded synchronously using the ultrahigh-speed camera with an exposure time of 5 ns. Six tests were performed with each laser energy, and then the average value was taken as the laser energy to excite the MFPs.

3. Results and Discussion

3.1. Layer Structure and Morphological Analysis of the MFPs. SEM images in a cross-sectional view of $Al/Al_2O_3/Al$ and $TiO_2/Al/Al_2O_3/Al$ were obtained to understand the internal structure and component of MFPs and showed an equiaxial block growth with a tightly bound layered structure in Figure 2. Al and dense Al_2O_3 contacted closely and were demarcated clearly. The thickness of $Al/Al_2O_3/Al$ (I) in each layer was 0.8 μm Al, 0.8 μm Al_2O_3, and 3.2 μm Al respectively; thus, a significant thickness and morphology difference can be seen among three layers from Figure 2(a). The SEM photograph of $Al/Al_2O_3/Al$ (II) with 0.4 μm Al, 0.4 μm Al_2O_3, and 2.6 μm Al in the comparison group also showed obvious boundary and dense layer structure. In addition, the SEM image of the energetic flyer plates $TiO_2/Al/Al_2O_3/Al$ (III) with 0.2 μm TiO_2, 0.2 μm Al, 0.4 μm Al_2O_3, and 2.6 μm Al also showed good compactness and clearly layered structure. The SEM analysis results showed that the internal structure and composition of the MFPs were the same as expected, indicating that the samples we prepared can be used as energy conversion microdevices with adjusted performance.

3.2. Energy Conversion Performance of MFPs. The dynamic process of laser-driven MFP acceleration was recorded simultaneously by the PDV system and ultrahigh-speed video. As shown in Figures 3 and 4, the time-velocity and time-displacement relationships of three types of flyer plates were obtained through the PDV system, and characteristic

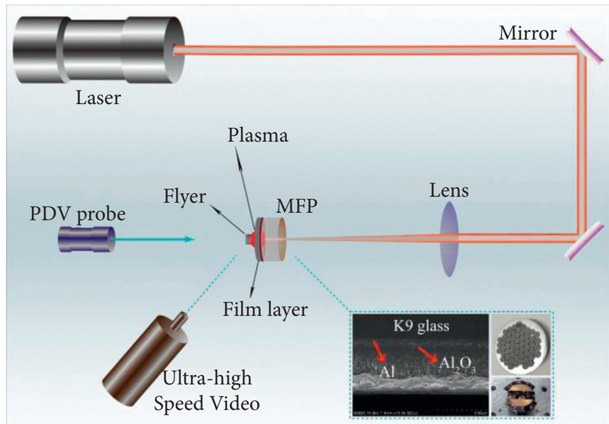

Figure 1: Schematic diagram of laser-driven MFPs.

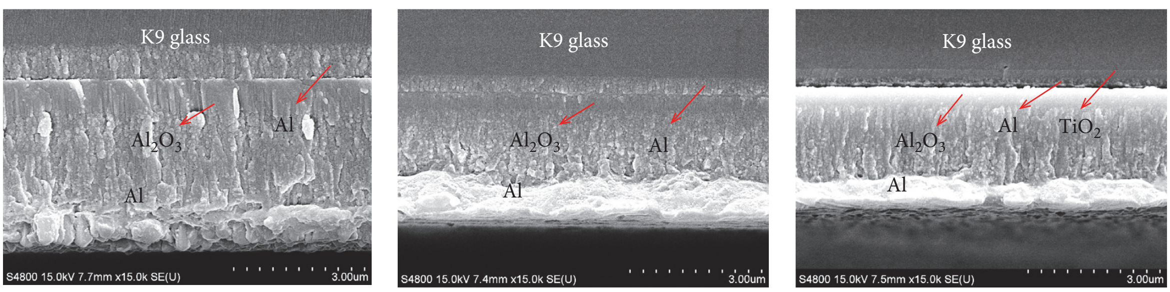

(a) (b) (c)

Figure 2: Cross-sectional SEM image of the MFPs. (a) $Al/Al_2O_3/Al$ (I). (b) $Al/Al_2O_3/Al$ (II). (c) $TiO_2/Al/Al_2O_3/Al$ (III).

velocity curves in different acceleration stages were observed. The velocity curves' variation of the flyer plates showed that the acceleration of the flyer plate can be divided into three stages: rapid acceleration stage, slow acceleration stage, and deceleration stage. The typical velocity curves of the flyer are shown in Figure 3, in which the excited laser energy was 43.1 J/cm^2. The rapid acceleration stage began when the flyer plate was driven away by the plasma and ended when the velocity increased to about three quarters of the final velocity. Rapid acceleration stage was characterized by a rapidly rising velocity of the flyer plate and the slowly decreasing acceleration, with a duration of about 20 ns. At the end of the rapid acceleration stage, the flyer entered the slow acceleration stage. The rising trend of the flyer velocity slowed down obviously at this time, and the acceleration decreased rapidly to zero. The slow acceleration stage lasted about three times as long as the rapid acceleration stage, which ended when the flyer plate reached the maximum velocity (final velocity). Finally, the flyer plate entered the deceleration stage, and its speed slowly decreased with the passage of time. It should be pointed out that, in the slow acceleration stage of $Al/Al_2O_3/Al$ (II) and $TiO_2/Al/Al_2O_3/Al$ (III), the phenomenon of flyer velocity bifurcation occurred, which was related to the material and structure of the flyer plates.

Figure 4 shows the velocity curves of three types of flyer plates over time. As can be seen, the three stages of the flyer plate acceleration process were clearly visible. For the rapid acceleration stage, the velocity of $Al/Al_2O_3/Al$ (I), $Al/Al_2O_3/Al$ (II), and $TiO_2/Al/Al_2O_3/Al$ (III) increased from 0 to 3500 m/s within 26 ns, 0 to 4100 m/s within 20 ns, and 0 to 4400 m/s within 24 ns, respectively, which was due to the high-pressure shock wave generated by the strong constrained expansion of the plasma plume at the initial moment when the flyer plate was sheared off. The shock wave formed by the rapid expansion of the plasma plume propagated back and forth in the Al flyer layer, which accelerated the flyer layer and made the velocity of the flyer plate rise very rapidly. At this time, the plasma just broke through the bound of the Al flyer layer from the confinement state and drove the flyer plate to accelerate rapidly in the barrel. However, the flyer plates moved about 55 μm, 46 μm, and 58 μm, respectively, in this stage, which accounted for 12.7%, 14.4%, and 20.7% of the displacement at the corresponding maximum velocity. From the velocity curve and flight distance, it can be concluded that the speed of the energetic flyer plate increased more dramatically in the rapid acceleration stage. When the velocity increased slowly in the barrel, the flight process of the flyer plate entered the second stage: slow acceleration stage. At this time, the acceleration of the flyer plate decreased rapidly, which reduced the velocity increment of the flyer plate. However, due to the high velocity level of the flyer plate and the long flight duration time, the flyer plate had a large displacement at this stage. At this stage, the maximum velocity of $Al/Al_2O_3/Al$ (I) reached 4201.0 m/s (432.7 μm flight distance), while the maximum

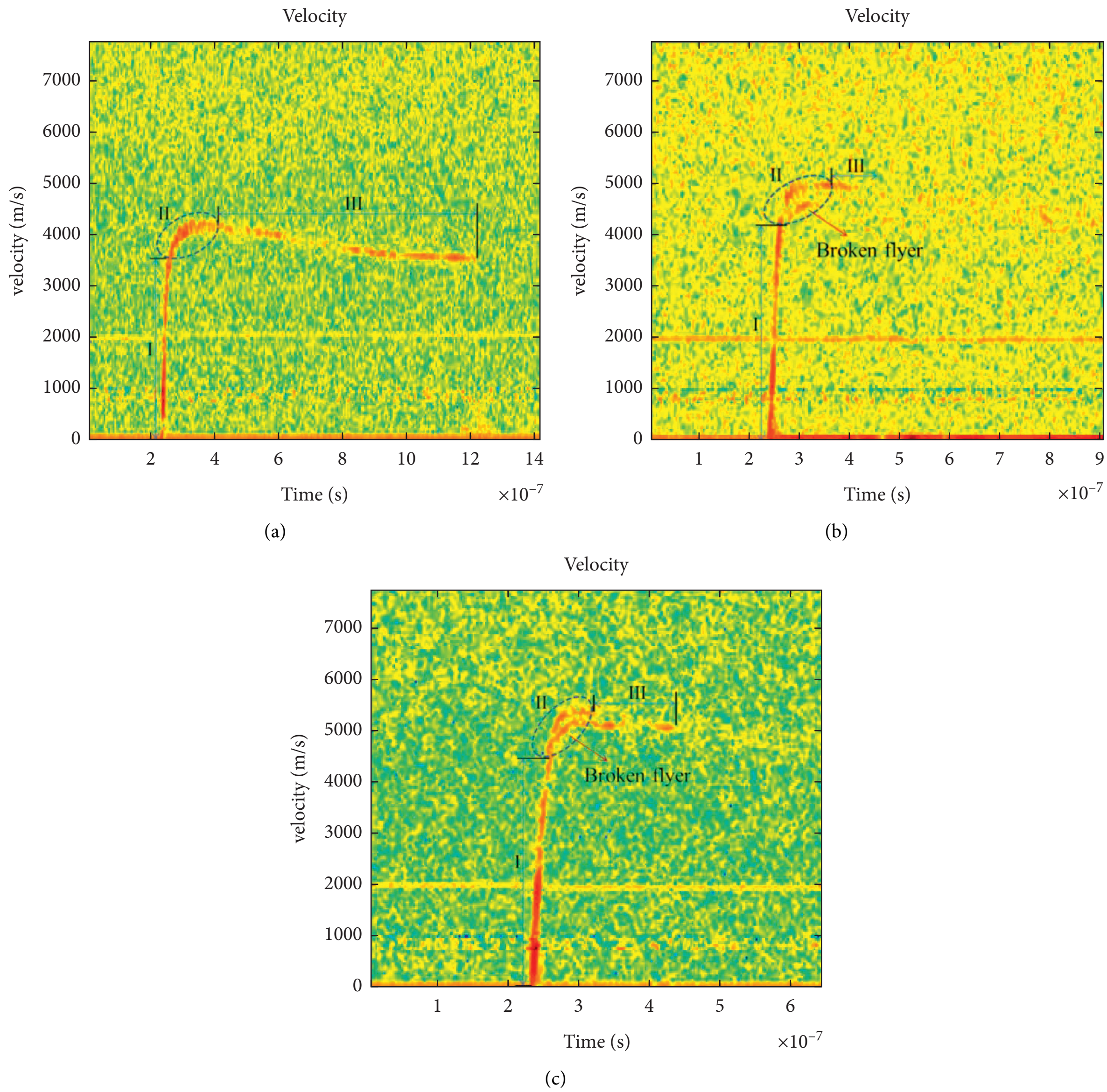

Figure 3: Time-velocity curves of MFPs with different types. (a) $Al/Al_2O_3/Al$ (I). (b) $Al/Al_2O_3/Al$ (II). (c) $TiO_2/Al/Al_2O_3/Al$ (III).

velocities of $Al/Al_2O_3/Al$ (II) after fragmentation were 4609.8 m/s (257.9 μm flight distance) and 4988.1 m/s (320.0 μm flight distance), and the maximum velocities of $TiO_2/Al/Al_2O_3/Al$ (III) after fragmentation were 5182.2 m/s (274.6 μm flight distance) and 5386.7 m/s (280.5 μm flight distance), respectively.

It can be inferred from the velocity variation curves of $Al/Al_2O_3/Al$ (II) and $TiO_2/Al/Al_2O_3/Al$ (III) in the slow acceleration stage that the flyer plate layer fragmentation occurred, as shown in Figures 3(b), 3(c), and 4(b), which did not appear in the rapid acceleration stage. As time goes by, the flyer flew in the slow acceleration stage which was constantly eroded by the high temperature and high pressure from the plasma plume and the shock wave. Due to the thin Al_2O_3 insulation thickness of the flyer plate, it was unable to effectively isolate the shock and ablation of the plasma plume. Therefore, the breakage phenomenon appeared at the weak point of the flyer layer, and the velocity differentiation occurred in the slow acceleration stage as shown in the velocity curve. Therefore, the thicker Al_2O_3 insulating layer can prevent the flyer plate from breaking under the shock and ablation of high-temperature and high-pressure plasma. During the slow acceleration stage, the reason for the slow increase of the flyer velocity was that the energy used to support the shock wave in the plasma plume became less. As the flyer plate was completely sheared, the plasma plume lost strong constraint, causing the plasma plume to expand very rapidly. The rapid expansion of the plume reduced the pressure of the plasma, resulting in a reduction in the pressure that drove the flyer plate. Therefore, the energy obtained by the shock wave in the flyer layer and the acceleration effect of the shock wave on the flyer were reduced, which was shown as the acceleration slowing down in the curve.

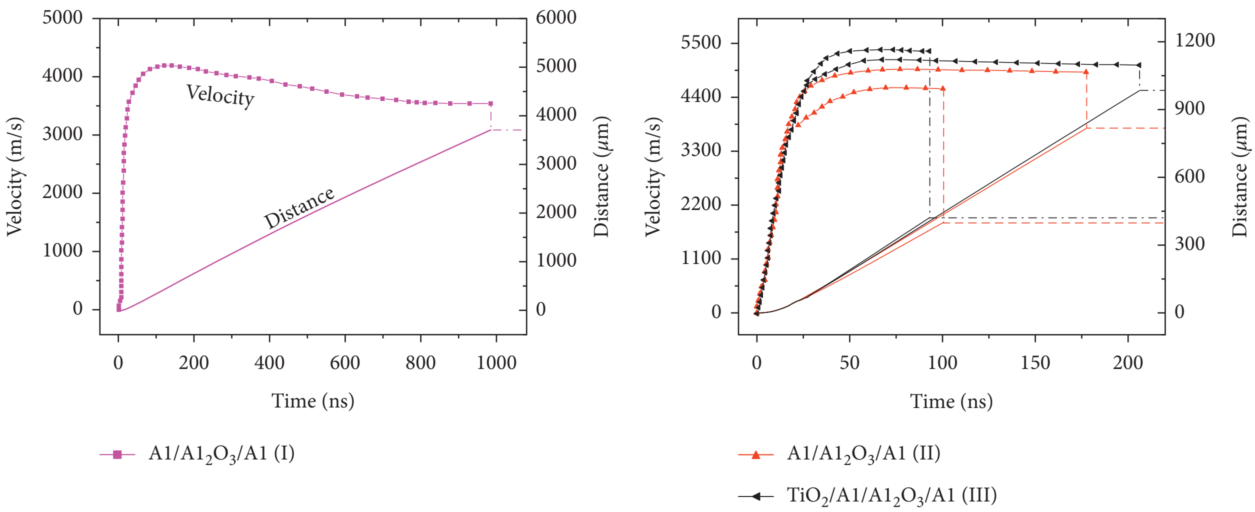

(a) (b)

FIGURE 4: Velocity and displacement histories of MFPs. (a) $Al/Al_2O_3/Al$ (I). (b) $Al/Al_2O_3/Al$ (II) and $TiO_2/Al/Al_2O_3/Al$ (III).

When the flyer plate reached its maximum velocity, the flight of the flyer plate moved from the second stage to the third stage: the deceleration stage. For the $Al/Al_2O_3/Al$ (I) flyer plate, the velocity of the flyer plate at this stage showed a trend of slow decline and lasted for a long time, reached about 776 ns, but the velocity of the flyer plate still remained at a high level. As a result, the total flight distance of the flyer plate reached 3.72 mm. As for the flyer plates of $Al/Al_2O_3/Al$ (II) and $TiO_2/Al/Al_2O_3/Al$ (III), the velocity evolution curves of the two types of flyer plates in the deceleration stage became shorter because the flyer plates were broken in the slow acceleration stage. Thus, the displacements of $Al/Al_2O_3/Al$ (II) and $TiO_2/Al/Al_2O_3/Al$ (III) reached only 817.2 μm and 984.9 μm, respectively. In addition, by reducing the thickness of the MFPs, the velocity of the flyer plate was also effectively improved, which was mainly caused by the reduction of the mass of the flyer plate. Among them, TiO_2/Al film as the ablative layer of MFPs had the highest final velocity, which was due to the increased heat release and laser absorption of the thermite system. It was also found that the sufficient insulation layer thickness of the flyer plate can improve effectively the integrity of the flyer plate so that the flyer plate can still remain intact when flight a long distance.

In order to more intuitively observe the morphologic changes of the flyer plate in the flight process, ultrahigh-speed photography was used to shoot the flight process of the three types of MFPs, and the results are shown in Figure 5. As can be seen from the figure, $Al/Al_2O_3/Al$ (I) maintained a relatively complete morphology under the plasma drive within 700 ns, which was due to its thick Al_2O_3 insulation layer that could effectively isolate the impact ablation of high-temperature and high-pressure plasma, while $Al/Al_2O_3/Al$ (II) and $TiO_2/Al/Al_2O_3/Al$ (III) were broken and separated under the impact ablation of the laser-induced plasma within 100 ns. These characteristics were consistent with the time-velocity curves of the three kinds of MFPs. $Al/Al_2O_3/Al$ (I) maintained a relatively complete appearance during the laser driving process, so the obtained time-velocity curve was relatively complete. However, the time-velocity curves of $Al/Al_2O_3/Al$ (II) and $TiO_2/Al/Al_2O_3/Al$ (III) showed a bifurcation phenomenon, and the duration was also shorter. These results indicated that the 0.4 μm-thick Al_2O_3 insulation layer cannot guarantee the integrity of the flyer plate, so the design of the insulation layer should be thicker with 43.1 J/cm^2.

3.3. *Probing the Pyrolysis Mechanism of TiO_2/Al.*

The MFPs based on the TiO_2/Al thermite film had the highest final velocity, which may be related to the laser absorption and the exothermic reaction of the thermite film. In order to verify the influence of the TiO_2/Al thermite film on the laser conversion efficiency of MFPs, the laser reflectivity was tested. Figure 6 shows the laser reflectivity of Al and TiO_2/Al films. It can be seen from the figure that the laser reflectivity of the Al film was between 80 and 90%, while that of TiO_2/Al was relatively low, between 70 and 80%. Under the irradiation of the 1064 nm laser, the laser reflectivity of the Al film was 80.55%, and that of TiO_2/Al was 72.13%. The absorptivity of the TiO_2/Al film to the 1064 nm laser was higher than that of the Al film, so it can be inferred that more laser energy was used as ablation.

The differential thermal analysis (DTA) instrument was used to characterize the exothermic behavior of the TiO_2/Al ablative layer at different heating rates (from 5 to 20°C/min) in order to obtain the energy release law of the films under thermal stimulation. The thermal analysis experiments were conducted to study the heat release of the TiO_2/Al layer under the N2 flow with the temperatures ranging from 30 to 900°C. As can be seen from Figure 7, the exothermic reaction of the TiO_2/Al film between 300 and 800°C was divided into two stages [22]. The remarkable exothermic peaks of TiO_2/Al were 653.19, 674.00, 692.95, and 702.43°C at heating rates from 5 to 20°C/min, respectively. The smaller exothermic peaks were shown at 345.64, 354.73, 384.85, and 393.14°C,

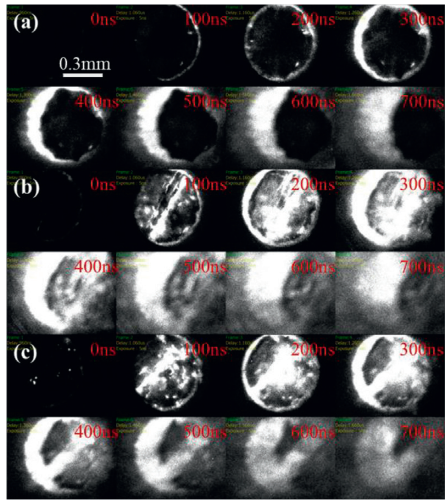

FIGURE 5: Ultrahigh-speed photography of the flight process for various flyer plates. (a) Al/Al2O3/Al (I). (b) Al/Al2O3/Al (II). (c) TiO_2/Al/Al_2O_3/Al (III).

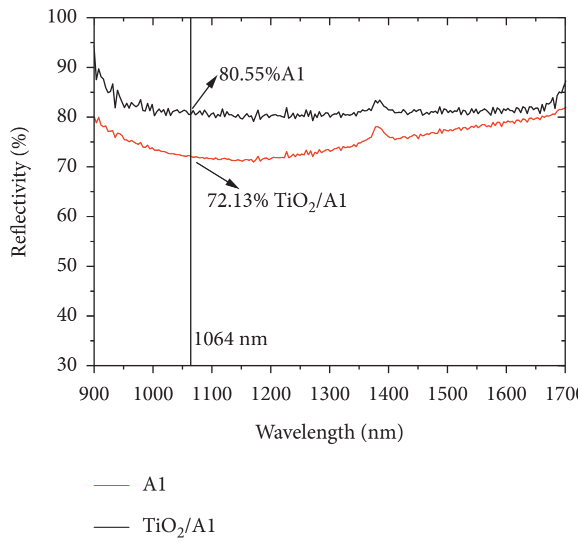

FIGURE 6: The laser reflectivity of ablation films.

corresponding to heating rates from 5 to 20°C/min, respectively. According to the heat release curves, the heat release in the high-temperature section was greater than that in the low-temperature section. With the decreased heating rate, the peak temperature and heat release of the exothermic reaction decreased. The Kissinger method was utilized to estimate the activation energy (Ea) of the two exothermic peaks of the TiO_2/Al film [22, 23]. The activation energy of the first exothermic peak was estimated to be 23.81 kJ/mol, while the activation energy reached 93.70 kJ/mol for the second exothermic peak, which was much higher than that of the first exothermic peak. With the decreased heating rates, the initial reaction temperature of the TiO_2/Al film decreased, which was consistent with the change of reaction process curves, as shown in Figure 8. The temperature range of the first exothermic peak of 30% conversion was 365–378°C, and that of the second exothermic peak of 30% conversion was 660–695°C.

The first exothermic reaction occurred in the ranges of 300–450°C before Al melted, at which time, the aluminothermic film released less heat. The results showed that the solid-solid diffusion reaction was most likely to occur in the interface layer between Al and TiO_2, as shown in Figure 9, which was attributed to the reduction of the diffusion distance between Al and TiO_2 layers prepared by magnetron sputtering, and the Al_2O_3 barrier layer formed between the film layers was thin or defective. The solid-solid reaction gradually formed a relatively complete Al_2O_3 barrier layer between the film layers, preventing Al and TiO_2 from further reacting. The second heat release peak occurred after Al melting (melting point of the Al film was 645°C), which was a solid-liquid reaction between liquid Al and solid TiO_2. Different from the reaction of the TiO_2/Al layer in the first stage, a relatively complete and thick Al_2O_3 barrier layer was formed between Al and TiO_2. As temperature rose, melted Al can partially break

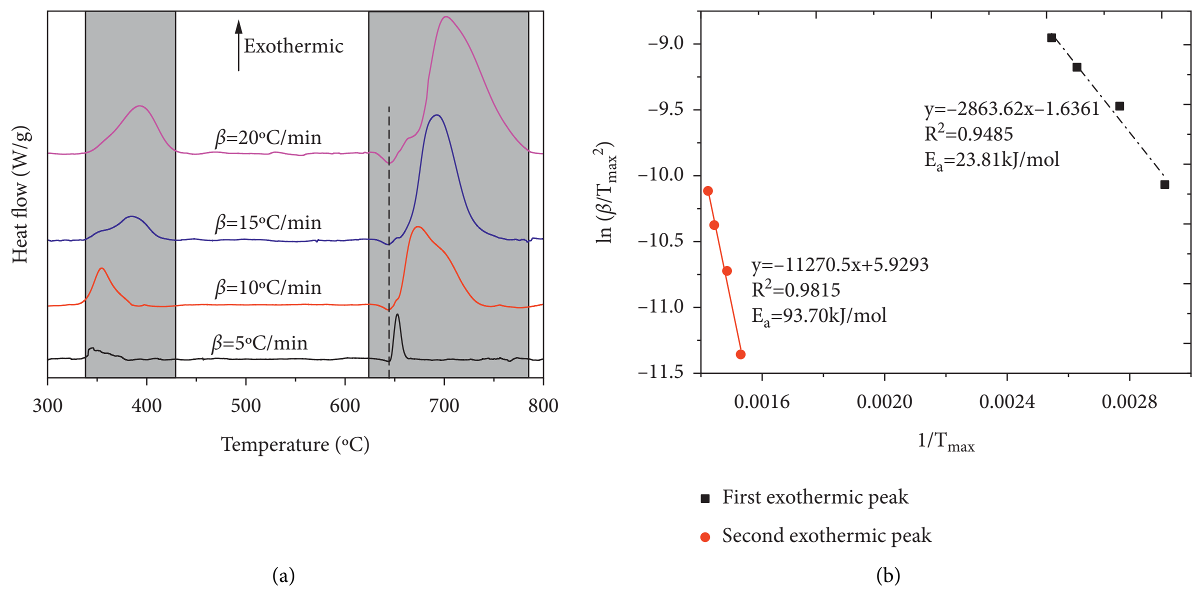

FIGURE 7: (a) The reaction exothermic curve and (b) the activation energy of TiO_2/Al.

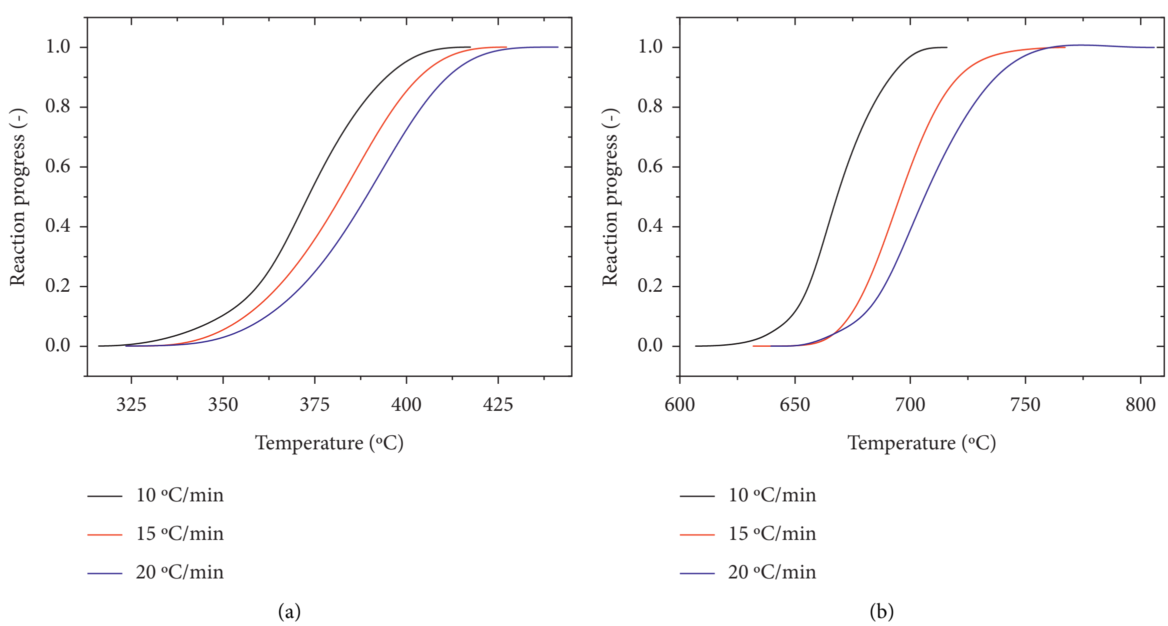

FIGURE 8: The reaction progress curves of the two exothermic peaks. (a) First exothermic peak. (b) Second exothermic peak.

the Al_2O_3 layer and flow out, resulting in the reaction with TiO_2. It can be inferred that the second exothermic peak as the main exothermic reaction was the result of the full reaction between melted Al and TiO_2.

The activation energies of the two exothermic peaks corresponded to the solid-solid and solid-liquid chemical reactions at two temperature stages, respectively, and also corresponded to the difficulty of the two reactions. The first solid-solid reaction between 300°C and 450°C was relatively easy to occur, while the second exothermic reaction required molten Al to break through the Al_2O_3 barrier layer; thus, two kinds of reaction mechanisms have been speculated for the TiO_2/Al film [20, 24–27]. The solid-solid reaction was condensed state of free molecular oxygen reaction process equation (1), in which free oxygen firstly reacted with Al and then produced the Al_2O_3 barrier in the interface. The solid-liquid reaction was gas state reaction process equation (2), in which molten Al breached the Al_2O_3 barrier layer and reacted with the decomposition oxygen molecules of the oxidizer.

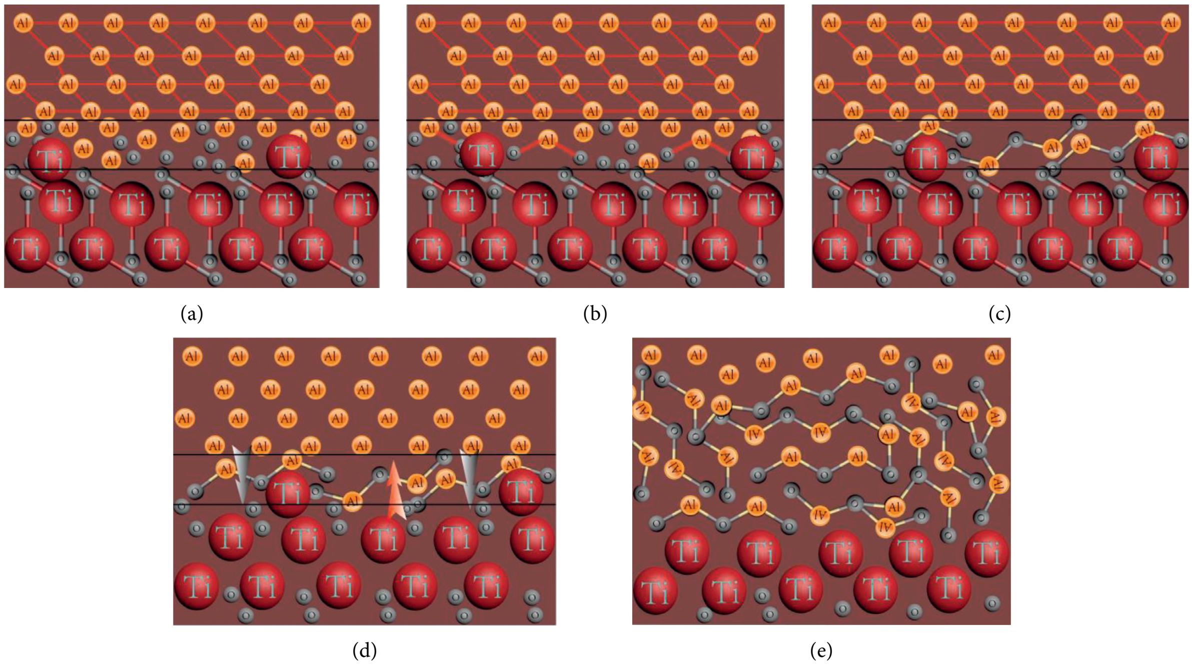

Figure 9: Schematics of the main reaction mechanism of the TiO_2/Al film. (a) As-deposited. (b) Solid-solid reaction. (c) Al_2O_3 barrier. (d) Molten Al. (e) Solid-liquid reaction.

$$\mathrm{Al} + \mathrm{O}_x \longrightarrow \mathrm{Al_2O_3}, \tag{1}$$

$$\begin{cases} \mathrm{MO}_x \longrightarrow \mathrm{MO}_{x-1} + \dfrac{1}{2}\mathrm{O}_2, \\ \mathrm{Al} + \mathrm{MO}_{x-1} \longrightarrow \mathrm{Al_2O_3} + \mathrm{M}. \end{cases} \tag{2}$$

In general, the energy release from the TiO_2/Al film under thermal stimulation contributed to the improvement of the output capacity of the system. Therefore, combined with the velocity of flyer plate results, it can be found that using the laser to stimulate a thermite reaction can also increase the energy of the plasma, thus improving the flyer output capacity. In addition, the peak temperature and heat release of the exothermic peak presented with increasing heating rate tended to increase. The second exothermic by the thermite film was higher than that of the first exothermic reaction.

4. Discussion

The energy was prestored in the ablation layer of the MFPs through the aluminothermic film. When the laser excited the MFPs, the stored energy will be used as one of the sources of plasma expansion and work, thereby increasing the total energy of MFPs [19, 28–30]. In addition, the introduction of the aluminothermic film reduced the reflectivity of the 1064 nm laser, which was conducive to the ablation layer film to absorb more laser energy, so as to improve the utilization efficiency of laser energy. However, due to the effect of high temperature and high pressure of the plasma, the thinner insulation layer was easily broken, which may result in a declined output performance of the MFPs. The MFPs with the aluminothermic film can reach the highest velocity, but in a short time, the flyer plate was broken and unable to fly long distances. Therefore, increasing the thickness of the insulating layer helped to improve the integrity of the flyer plate in the MFP design. For example, TiO_2/Al/Al_2O_3/Al (III) with a thickness of 0.4 μm Al_2O_3 ensured an integrity flight of 65 μm (in less than 25 ns) with the 43.1 J/cm^2 laser, while the insulation layer of 0.8 μm Al_2O_3 protected the integrity of Al/Al_2O_3/Al (I) throughout the flight. If the thickness of the Al_2O_3 insulation layer is increased, the integrity of the flyer will be improved. So, in combination with the specific service environment, proper adjustment of the structure and materials of each layer can improve the output capability while guaranteeing the integrity of the flyer plate.

5. Conclusions

In this study, nonenergetic Al/Al_2O_3/Al and energetic TiO_2/Al/Al_2O_3/Al MFPs were prepared by magnetron sputtering, and the films were uniform and compact without defects. Photon Doppler velocity system and ultrahigh-speed photography were used to characterize the flight characteristics of the flyer plate. Flyer velocity curves, displacement curves, flight images, and other information were used to analyze the output performance of flyer plates. The results showed that the acceleration process of the laser-driven flyer plate can be divided into three stages: rapid acceleration stage, slow acceleration stage, and deceleration stage. Sufficient oxide layer thickness of Al/Al_2O_3/Al (I) can effectively protect the integrity of the flyer plates, but the flyer velocity was reduced to 4201.0 m/s. When the film thicknesses were reduced, the velocities of Al/Al_2O_3/Al (II) and TiO_2/Al/

Al_2O_3/Al (III) were increased to 4988.1 m/s and 5386.7 s m/s, respectively, but both of them were broken in the slow acceleration stage. In addition, the low laser reflectivity and reaction heat release of the thermite film improved the final flight velocity of the energetic flyer plate, which can facilitate the practical ignition and initiation applications of laser driving technology.

Data Availability

The data that support the findings of this study are available from the corresponding author upon reasonable request.

Conflicts of Interest

The authors declare no conflicts of interest.

Acknowledgments

This work was supported by the Cultivation Project of Innovation and Development Foundation of CAEP (PY20210024) and the Subject Project of ICM (SXK-2021-19). The authors wish to thank Zhiwei Han and Ningxi Meng for their constructive advice.

References

[1] P. Krehl, F. Schwirzke, and A. W. Cooper, "Correlation of stress-wave profiles and the dynamics of the plasma produced by laser irradiation of plane solid targets," *Journal of Applied Physics*, vol. 46, no. 10, pp. 4400–4406, 1975.

[2] H. Xiuguang, F. Sizu, G. Yuan et al., "The research of a method of absolute measurement for laser-driven high pressure equation of state," *Acta Physica Sinica*, vol. 51, pp. 337–341, 2002.

[3] K. Okada, K. Wakabayashi, H. Takenaka et al., "Experimental technique for launching miniature flying plates using laser pulses," *International Journal of Impact Engineering*, vol. 29, no. 1-10, pp. 497–502, 2003.

[4] A. A. Banishev, W. L. Shaw, W. P. Bassett, and D. D. Dlott, "High-speed laser-launched flyer impacts studied with ultrafast photography and velocimetry," *Journal of Dynamic Behavior of Materials*, vol. 2, no. 2, pp. 194–206, 2016.

[5] H. Liu, H. Wang, Z. Shen et al., "The research on micropunching by laser-driven flyer," *International Journal of Machine Tools and Manufacture*, vol. 54-55, pp. 18–24, 2012.

[6] M. Bowden, M. P. Maisey, and S. Knowles, "Shock initiation of hexanitrostilbene at ultrahigh shock pressures and critical energy determination," *AIP Conference Proceedings*, vol. 1426, pp. 615–618, 2012.

[7] D. L. Paisley, *Laser-driven Miniature Flyer Plates for Shock Initiation of Secondary Explosives*, Los Alamos National Lab., Los Alamos, NM, USA, 1989.

[8] R. E. Setchell, "Grain-size effects on the shock sensitivity of hexanitrostilbene (HNS) explosive," *Combustion and Flame*, vol. 56, no. 3, pp. 343–345, 1984.

[9] M. D. Bowden, *The Development of a Laser Detonator System*, Cranfield University, Cranfield, England, 2015.

[10] X. H. Zhao, Y. Gao, and X. Zhao, "Development of laser initiation technology," *Infrared and Laser Engineering*, vol. 38, pp. 797–802, 2009.

[11] H. Y. Wang, E. Y. Chu, A. F. He, C. Jianhua, and J. Bo, "The research on the flyer film parameters for the initiation of HNS-IV by laser-driven flyer," *Initiators Pyrotech*, vol. 1, pp. 44–47, 2015.

[12] S. W. Dean, F. C. De Lucia, and J. L. Gottfried, "Indirect ignition of energetic materials with laser-driven flyer plates," *Applied Optics*, vol. 56, no. 3, pp. B134–B141, 2017.

[13] H. Zhang, L. Wu, P. Hu et al., "Launch and impact characteristics of typical multi-layered flyers driven by ns-pulsed laser," *Optics & Laser Technology*, vol. 120, Article ID 105709, 2019.

[14] Z. H. Wang, Y. Li, W. Z. Qin et al., "Research progress in the flight characteristics of laser-driven flye," *Chinese Journal of Energetic Materials*, vol. 27, pp. 255–264, 2019.

[15] W. Z. Qin, Z. H. Wang, B. He, G. Yuan, W. Yao, and W. Liang, "Influence of barrel parameters on velocity and morphology of laser-driven flyer," *Chinese Journal of Energetic Materials*, vol. 28, pp. 99–104, 2020.

[16] M. D. Bowden and R. Drake, *The initiation of high surface area Pentaerythritol Tetranitrate using fiber-coupled laser-driven flyer plates*, Optical Technologies for Arming, Safing, Fuzing, and Firing III, San DIego, CA, USA, 2007.

[17] S. Chen, L. Wu, R. Shen, Y. Ye, and T. Hua, "Laser-driven performance of the Al/Al2O3/Al multi-layer flyer," *Laser Physics*, vol. 23, no. 12, Article ID 125002, 2013.

[18] S. Chen, L. Wu, R. Shen, Y. Ye, and Y. Hu, "Initiation of HNS-IV using a laser-driven multi-layer flyer," *Baozha Yu Chongji*, vol. 35, pp. 285–288, 2015.

[19] Z. Shenghua, W. Lizhi, C. Shaojie et al., "Preparation and characteristics of laser-driven energetic composite flyer, high power laser part," *Beams*, vol. 27, Article ID 013, 2015.

[20] W. Guo, L. Wu, N. Meng et al., "Optimisation of modulation period of TiO2/Al reactive multilayer films for laser-driven flyer plates," *Chemical Engineering Journal*, vol. 360, pp. 1071–1081, 2019.

[21] W. Guo, L. Wu, N. He et al., "Efficiency relationship between initiation of HNS-IV and nanosecond pulsed laser-driven flyer plates of layered structure," *Laser and Particle Beams*, vol. 36, no. 1, pp. 29–40, 2018.

[22] W. Guo, S. Chang, J. Cao, L. Wu, R. Shen, and Y. Ye, "Precisely controlled reactive multilayer films with excellent energy release property for laser-induced ignition," *Nanoscale Research Letters*, vol. 14, no. 1, Article ID 301, 2019.

[23] V. P. Sinditskii, A. V. Burzhava, and A. B. Sheremetev, "Macrocyclic tetra(azo-) and tetra(azoxyfurazan)s: comparative study of decomposition and combustion with linear analogs," *Energetic Materials Frontiers*, vol. 2, no. 2, pp. 87–95, 2021.

[24] K. Zhang, C. Rossi, P. Alphonse, C. Tenailleau, S. Cayez, and J.-Y. Chane-Ching, "Integrating Al with NiO nano honeycomb to realize an energetic material on silicon substrate," *Applied Physics A*, vol. 94, no. 4, pp. 957–962, 2009.

[25] I. Abdallah, J. Zapata, G. Lahiner et al., "Structure and chemical characterization at the atomic level of reactions in Al/CuO multilayers," *ACS Applied Energy Materials*, vol. 1, no. 4, pp. 1762–1770, 2018.

[26] J. Dai, J. Xu, F. Wang et al., "Facile formation of nitrocellulose-coated Al/Bi 2 O 3 nanothermites with excellent energy output and improved electrostatic discharge safety," *Materials & Design*, vol. 143, pp. 93–103, 2018.

[27] J. Xu, Y. Shen, C. Wang et al., "Controlling the energetic characteristics of micro energy storage device by in situ deposition Al/MoO3 nanolaminates with varying internal structure," *Chemical Engineering Journal*, vol. 373, pp. 345–354, 2019.

[28] M. Zhipeng, S. Qunrong, C. Qiang et al., “Laser ablation characteristic research of TiO2/Al energetic multilayer films,” *Explosive Materials*, vol. 46, pp. 6–11, 2017.

[29] R. Shen, L. Wu, W. Zhang, and H. Zhang, “Laser ablation of energetic materials,” in *Laser Ablation-From Fundamentals to Applications*, T. Itina, Ed., InTech open, London, UK, pp. 259–279, 2017.

[30] W. Yao, Q. WenZhi, L. Yong, T. Duo, and W. Liang, “Al/Ni reactive multilayer films enhancing the properties of plasma induced by nanosecond pulsed laser,” *Energ. Mater. Front.*vol. 2, pp. 147–153, 2021.